ARTICLE

Expanding and understanding the CRISPR toolbox for *Bacillus subtilis* with MAD7 and dMAD7

Marcus A. Price[1] 🄿 | Rita Cruz[2] | James Bryson[3] | Franck Escalettes[2] | Susan J. Rosser[1,3,4] 🄿

[1]School of Biological Sciences, Institute of Quantitative Biology, Biochemistry, and Biotechnology, University of Edinburgh, Edinburgh, UK

[2]Molecular Biology Department, Ingenza Ltd., Roslin Innovation Centre, Roslin, UK

[3]School of Biological Sciences, UK Centre for Mammalian Synthetic Biology, University of Edinburgh, Edinburgh, UK

[4]Centre for Synthetic and Systems Biology and UK Centre for Mammalian Synthetic Biology, School of Biological Sciences, University of Edinburgh, Edinburgh, UK

Correspondence
Marcus A. Price, and Susan J. Rosser, School of Biological Sciences, Institute of Quantitative Biology, Biochemistry, and Biotechnology, University of Edinburgh, Edinburgh, UK.
Email: M.A.Price-4@sms.ed.ac.uk (M. A. P.) and Susan.Rosser@ed.ac.uk (S. J. R.)

Funding information
The Industrial Biotechnology Innovation Center (IBioIC), Grant/Award Number: PhD Studentship for M.A.P.

Abstract

The CRISPR-Cas9 system has become increasingly popular for genome engineering across all fields of biological research, including in the Gram-positive model organism *Bacillus subtilis*. A major drawback for the commercial use of Cas9 is the IP landscape requiring a license for its use, as well as reach-through royalties on the final product. Recently an alternative CRISPR nuclease, free to use for industrial R&D, MAD7 was released by Inscripta (CO). Here we report the first use of MAD7 for gene editing in *B. subtilis*, in which editing rates of 93% and 100% were established. Additionally, we engineer the first reported catalytically inactive MAD7 (dMAD7) variant (D877A, E962A, and D1213A) and demonstrate its utility for CRISPR interference (CRISPRi) at up to 71.3% reduction of expression at single and multiplexed target sites within *B. subtilis*. We also confirm the CRISPR-based editing mode of action in *B. subtilis* providing evidence that the nuclease-mediated DNA double-strand break acts as a counterselection mechanism after homologous recombination of the donor DNA.

KEYWORDS
Bacillus subtilis, Cas9, CRISPR, homologous recombination, MAD7

1 | INTRODUCTION

In recent years, precise genome editing with clustered regularly interspaced short palindromic repeats (CRISPR)-associated (Cas) systems have become widely used in many fields of biology (Jinek et al., 2012), enabling significant advances in genome editing tools for industrially relevant microorganisms, such as *Bacillus subtilis* (Altenbuchner, 2016; Burby & Simmons, 2017; Price, Cruz, Baxter, Escalettes, & Rosser, 2019; Westbrook, Moo-Young, & Chou, 2016b). Since the adaptation of the type II CRISPR-Cas9 system from *Streptococcus pyogenes* in 2012 for genomic engineering, along with subsequent iterations—including but not limited to CRISPR interference (CRISPRi) and CRISPR activation systems—it has become the most broadly utilized CRISPR based system in prokaryotes and eukaryotes (Altenbuchner, 2016; Burby & Simmons, 2017; Dicarlo

et al., 2013; Jakočiūnas, Jensen, & Keasling, 2015; Jakutyte-Giraitiene & Gasiunas, 2016; Jinek et al., 2012; Lu et al., 2019; Peng et al., 2017; Peters et al., 2016; Price et al., 2019; Westbrook et al., 2016b; K. Zhang, Duan, & Wu, 2016; Zhu et al., 2017). Cas9 induces a blunt DNA double-strand break (DSB) when in complex with either a two-component crRNA–tracrRNA or where these are combined into a single guide RNA complex (Jinek et al., 2012). Previous literature describes that once the DSB is introduced, it can be repaired by nonhomologous end-joining (NHEJ), or by homology directed repair (HDR) when a donor template DNA (dDNA) is supplied (Adli, 2018; Altenbuchner, 2016; Burby & Simmons, 2017; Jinek et al., 2012; Westbrook, Moo-Young, & Chou, 2016a). The inefficiency or total lack of an NHEJ system within most bacteria limits the choice for repair of the cut to HDR in most of these hosts (Shuman & Glickman, 2007).

CRISPRi in bacteria functions through the targeting of a catalytically inactive (D10A and H840A) Cas9 variant, dCas9 to the promoter or within the 5′ region of a gene of interest. This sterically hinders transcription by the RNA polymerase, thus lowering the successful expression of the target gene (Qi et al., 2013). CRISPRi has been exemplified within the Gram-positive model organism *Bacillus subtilis* (Westbrook et al., 2016b), perhaps most notably by Peters et al. (2006) for the functional analysis of all essential genes.

An alternative CRISPR nuclease family, Cpf1 (also known as Cas12a), has similarly been used for genome editing since the first report in 2015 (Zetsche et al., 2015). Cpf1 nucleases exhibit different characteristics to Cas9 nucleases, such as a staggered DSB, a T-rich PAM and the native use of only 1 guide RNA molecule to form a complex with Cpf1 and target the DNA. These characteristics enable Cpf1 nucleases to be used in target organisms or regions within an organism's genome were a lower GC content makes the use of Cas9 less feasible.

While the commercial application of Cas9 nucleases, and increasingly also Cpf1 nucleases, have been widely pursued, a significant drawback for the use of these nucleases is the requirement of a research license and potentially subsequent royalty fees for the commercial exploitation of any developed product.

Recently, Inscripta (CO) released the alternative CRISPR nuclease MAD7 which is free for all commercial or academic research with no reach-through royalties or costs provided the final engineered strain does not contain the MAD7 nuclease (Inscripta, 2019b). As such, its use for commercial genome editing is of great interest. Inscripta report that MAD7 was developed from *Eubacterium rectale* and has proven its functionality in *E. coli*, *S. cerevisiae* and in the human HEK293T cell line. Recently, MAD7 (also known as ErCas12a) was shown to be compatible with genome editing in Zebrafish (Wierson et al., 2019). MAD7 has 31% identity with *Acidaminococcus sp.* BV3L6 Cpf1 (AsCpf1), to which it also shares a T-rich PAM site (5′-YTTN-3′), and a protospacer (the region of the gRNA which associates the nuclease to the DNA target) length of 21 nucleotides (Inscripta, 2019a). A catalytically inactive variant of MAD7 has the potential to be combined with inactive dCas9 and/or ddCpf1 based tools to enable the construction of increasingly sophisticated synthetic biology genetic circuits.

Several CRISPR genome modification systems have been reported for use in the Gram-positive model organism *Bacillus subtilis* based around the efficient homologous recombination (HR) machinery, all of which utilize the Cas9 nuclease (Altenbuchner, 2016; Burby & Simmons, 2017; Price et al., 2019; Westbrook et al., 2016b; K. Zhang et al., 2016), or recently also the partially inactivate nCas9 (D10A) (Liu et al., 2019). Here we demonstrate that CRISPR-Cas9 genome editing in *B. subtilis* 168 is driven primarily by HR by curing *B. subtilis* 168 tryptophan auxotrophy. Subsequently, we show editing with MAD7 is also driven primarily by HR. We used the reporter proteins, AmyE and GFPmut3, to analyze the editing efficiency of this CRISPR-MAD7 system and engineered MAD7 to generate the first reported catalytically inactive, "dead," MAD7 (dMAD7) for single target and multiplexed transcriptional downregulation by dMAD7-mediated CRISPRi.

2 | MATERIALS AND METHODS

2.1 | Strains and media

The strains and plasmids used in this study are listed in Table S1. All oligonucleotides used in this study are listed in Table S2. *Escherichia coli* Top10 cells were used to construct recombinant plasmids. Bacterial cells were cultured in Lysogeny broth (LB) broth or LB agar (VWR) media at 37°C with agitation (250 rpm) where appropriate. *B. subtilis* 168 tryptophan auxotrophy or prototrophy were selected for by growth on M9 agar supplemented with or without 20 μg/mL tryptophan (Harwood & Cutting, 1990). When required, the following antibiotics were supplied to the media: ampicillin (200 μg/mL), chloramphenicol (10 μg/mL), and kanamycin (*E. coli*: 100 μg/mL; *B. subtilis*: 10 μg/mL).

2.2 | Plasmid and strain construction

Unless otherwise stated, plasmid construction was performed as described in Sambrook and Russell (2001). DNA oligonucleotides were purchased from Merck or Integrated DNA Technologies. The reagents for polymerase chain reaction (PCR), restriction digest, DNA phosphorylation, and ligation were purchased from New England Biolabs (NEB). DNA purification was performed using the Monarch® Nucleic Acid Purification Kits from NEB. DNA sequences were confirmed by Source Bioscience.

2.2.1 | CRISPR plasmid construction

pBAC0155 was constructed using the inABLE plasmid assembly method (Che, Knight, Canton, Kelly, & Shetty, 2015; Price et al., 2019). Individual 5′ truncated parts were prepared by PCR followed by restriction digest at 5′ and 3′ regions with SapI. Where parts <120 base pair (bp) were used, complementary oligonucleotides were phosphorylated and annealed leaving three nucleotides (nts) single strands at both the 5′ and 3′ ends to remove the need for SapI digestion. The parts were ligated to phosphorylated and annealed oligonucleotides at each terminus, containing 3 nt and 16 nt single strands at the 5′ and 3′ ends, respectively. The part- oligonucleotides fusions were annealed at the homologous 16 nt overhangs for 1 hr at 37°C, and used to transform electrocompetent *E. coli*.

pBAC0155 consisted of four parts: 1. the *E. coli/B. subtilis* shuttle vector backbone from pBAC0001; 2. the LacI repressor and isopropyl β-D-1-thiogalactopyranoside (IPTG) inducible P*grac* promoter from pBAC0001, including a multiple cloning site; 3. the bidirectional strong *rrnB* T1 and T2 terminators; 4. the MAD7 gRNA expression module consisting of the P*veg* promoter, the "MAD7 handle" section of the gRNA and spacer DNA flanked by SapI sites for cloning of the protospacer DNA. Three 5′ truncated parts were prepared by PCR from the indicated template and oligonucleotides: 1. pBAC0001 with oMAP0010/0011; 2. pBAC0001 with oMAP0018/0019; 3. pING0001

with oMAP0024/0025. The short part 4 was prepared as described from oMAP0492/0493. Parts were ligated at 5′ and 3′ respectively with annealed oligonucleotides: 1. oMAP0008/0009 and oMAP0014/0015; 2. oMAP0016/0017 and oMAP0020/0021; 3. oMAP0022/0023 and oMAP0486/0487; 4. oMAP0488/0489 and oMAP0498/0499.

pBAC0158 was constructed by digesting pBAC0155 and pMK-RQ-MAD7 (MAD7, codon-optimized for *B. subtilis* and flanked by BamHI and XbaI recognition sites, synthesized by Thermo Fisher Scientific) with BamHI and XbaI restriction enzymes, and ligating the pBAC0155 backbone with the *MAD7* gene using T4 DNA ligase.

pBAC0184, pBAC0194, and pBAC0195 were constructed by PCR amplifying dCas9 from pdCas9-bacteria with oligonucleotides oMAP0073/0074, introducing a BsaI site and XbaI recognition sites at the 5′ and 3′ end of the gene, respectively. The amplified *dcas9* was digested with BsaI and XbaI. pBAC0041, pBAC0035, and pBAC0165 were digested with BamHI and XbaI to remove the *cas9* gene. The *dcas9* gene fragment was subsequently ligated with the pBAC0041/0035/0165 backbones using T4 DNA ligase. pdCas9-bacteria was a gift from Stanley Qi (plasmid #44249; Addgene; Qi et al., 2013).

pBAC0187, pBAC0188, pBAC0189, and pBAC0190 were constructed by digesting pBAC0158, pBAC0162, pBAC0163, and pBAC0166, respectively, as well as pMK-RQ-dMAD7 (dMAD7 [MAD7 gene with D877A [codon GCT to GAT], E962A [codon GCA to GAA], D1213A [codon GCT to GAT] modifications] flanked by BamHI and XbaI recognition sites, synthesised by Thermo Fisher Scientific), with BamHI and XbaI. The *dMAD7* gene fragment was subsequently ligated with the pBAC0158/0162/0163/0166 backbones using T4 DNA ligase.

The protospacer insertion into pBAC0015, for the completion of Cas9-mediated genome editing plasmids, was carried out as previously described (Price et al., 2019). The construction of CRISPR plasmids for MAD7 or dMAD7 was carried out in a similar fashion, however SapI, instead of AarI, was used to cleave the pBAC0158 and pBAC0187 backbones to yield 3 nt single-stranded DNA overhangs compatible with the gRNA protospacer constructed by annealing of an oligonucleotide pair. All protospacer regions were identified using the online tool, CHOPCHOP (Labun, Montague, Gagnon, Thyme, & Valen, 2016; Montague, Cruz, Gagnon, Church, & Valen, 2014).

The following plasmids for Cas9-mediated editing were prepared with the pBAC0015 backbone using the indicated oligonucleotide pairs: pBAC0129 (oMAP0386/0387); pBAC0165 (oMAP0573/0574); pBAC0185 (oMAP0694/0695). The following plasmids for MAD7-mediated editing were prepared from the pBAC00158 backbone using the indicated oligonucleotide pairs: pBAC0162 (oMAP0549/0550); pBAC0163 (oMAP0553/0554); pBAC0166 (oMAP0571/0572); pBAC0218 (oMAP0799/0800). The following plasmids where prepared from the pBAC0187 backbone using the indicated oligonucleotide pairs: pBAC0207 (oMAP0759/0760); pBAC0208 (oMAP0761/0762); pBAC0209 (oMAP0763/0764); pBAC0210 (oMAP0765/0766); pBAC0211 (oMAP0767/0768); pBAC0212 (oMAP0769/0770); pBAC0213 (oMAP0771/0772); pBAC0214 (oMAP0775/0776); pBAC0215 (oMAP0777/0778); pBAC0219 (oMAP0793/0794); pBAC0220 (oMAP0797/0798); and pBAC0222 (oMAP0795/0796).

Schematic representations of plasmids pBAC0015, pBAC0155, pBAC0158, and pBAC0187 can be found in the supplementary information.

2.2.2 | dDNA preparation

dDNA, encoding a programmed target site edit together with a synonymous PAM mutation to eliminate Cas9 or MAD7 cleavage at the edited site after HR or HDR was constructed by overlap extension PCR (OE-PCR) as described previously (Bryksin & Matsumura, 2010; Price et al., 2019).

2.2.3 | Strain construction

BAC0111 was constructed by transforming naturally competent *B. subtilis* 168 with the integration plasmid pGFPbglS (Anagnostopoulos & Spizizen, 1961; Bennallack, Burt, Heder, Robison, & Griffitts, 2014; Bisicchia, Botella, & Devine, 2010). Transformants were selected on LB agar plates supplemented with kanamycin (Figure S1).

A total of 1 μg of an OE-PCR product generated using the oligonucleotides set oMAP0388/0393/0394/0395 and the genomic DNA (gDNA) of strain BAC0111 as template was co-transformed alongside 200 ng of the editing plasmid pBAC0129 for the modification of BAC0111 to insert P_{veg} upstream of *gfpmut3*. The editing plasmid was removed from the edited strain by overnight growth in LB supplemented with 1 mmol/L IPTG and subsequent confirmation by counter plating on LB agar plates with and without chloramphenicol, yielding strain BAC0288 (Figure S1; Price et al., 2019). The insertion of P_{veg} was verified by sequencing and by fluorescence emission analysis using Safe Imager 2.0 Blue Light Transilluminator and Amber Filter System (excitation: 470 nm, emission: 530 nm; Thermo Fisher Scientific) to detect GFPmut3.

BAC0348-0355 and BAC0360-0368 were constructed by transforming naturally competent cells of the relevant parental strain with the appropriate plasmid (Table S1; Anagnostopoulos & Spizizen, 1961; Bennallack et al., 2014). Transformants were selected on LB agar plates supplemented with chloramphenicol.

2.3 | CRISPR-Cas9/MAD7-Mediated gene editing in *B. subtilis*

A single OE-PCR product was used to allow a direct comparison between Cas9 and MAD7 editing efficiencies at the *amyE* locus. The OE-PCR product generated using the oligonucleotide set oMAP0121/0551/0552/0122 was co-transformed alongside the editing plasmids pBAC0041 and pBAC0162.

dDNA for *gfpmut3* editing was generated by PCR using oligos oMAP0575/0578 and the synthesized plasmid pMK-RQ-gfpmut3-dDNA as a template.

Genome editing was carried out in triplicate by co-transforming naturally competent *B. subtilis* with 200 ng editing plasmid DNA and 1 μg

dDNA (Anagnostopoulos & Spizizen, 1961; Bennallack et al., 2014; Price et al., 2019). When targeting *gfpmut3*, transformants were spread on LB agar plates supplemented with chloramphenicol and IPTG (1 mmol/L). Effective knock-out of *gfpmut3* by stop codon introduction was determined by analysis of fluorescence emission using Safe Imager 2.0 Blue Light Transilluminator and Amber Filter System (excitation: 470 nm; emission: 530 nm; Thermo Fisher Scientific). Genotypes were confirmed by colony PCR with oligonucleotides hybridizing to the chromosome (oMAP0393/0814) outside of the dDNA homology arm region and sequenced with primer oMAP0815 to ensure accurate coverage of the targeted region. When targeting *amyE*, transformants were spread on LB agar plates supplemented with chloramphenicol, IPTG (1 mmol/L) and 1% soluble potato starch (VWR). Effective knock-out of *amyE* by stop codon introduction was determined by staining transformation plates with iodine (Price et al., 2019; Zhang, Yan, Cui, Hong, & Li, 2006). Genotypes were confirmed by colony PCR with oligonucleotides hybridizing to the chromosome (oMAP0811/0812) outside of the dDNA homology arm region and sequenced with primer oMAP0813 to ensure accurate coverage of the targeted region.

2.4 | Restoring *B. subtilis* tryptophan prototrophy

The CRISPR-Cas9 genome editing mechanism in *B. subtilis* was investigated by restoring tryptophan prototrophy when transforming an OE-PCR product (oligonucleotides set oMAP0236/0696/0697/0239 and gDNA of *B. subtilis* 168 as template) containing the mutation needed to remove the *trpC2* lesion, in the presence and absence of editing plasmid pBAC0185, or Nontargeting plasmid pBAC0035 (Altenbuchner, 2016). Transformations were carried out in triplicate in naturally competent *B. subtilis* as previously described, and tryptophan prototroph cells were selected in M9 minimal medium (Anagnostopoulos & Spizizen, 1961; Bennallack et al., 2014; Price et al., 2019). Before spreading transformants on M9 agar plates, the cells were washed three times with 10 mmol/L phosphate-buffered saline to ensure there was no carryover of tryptophan from the transformation process.

The CRISPR-MAD7 genome editing mechanism in *B. subtilis* was investigated in the same manner. OE-PCR product (oligonucleotides set oMAP0236/0801/0802/0239 and gDNA of *B. subtilis* 168 as template) containing the mutation needed to remove the *trpC2* lesion was transformed in the presence and absence of editing plasmid pBAC0218, or nontargeting plasmid pBAC0163. IPTG was included in all transformation plates to limit the background of nonselected colony forming units (CFUs).

Transformation results between different batches of competent cells were normalized by the transformation efficiency obtained when transforming only the nontargeting plasmid for the nuclease being analyzed and selecting on LB agar supplemented with chloramphenicol (Cas9), or LB agar supplemented with chloramphenicol and IPTG (MAD7).

Unpaired *t* tests with Welch's correction were performed to determine two-tailed *p* values and identify statistically significant or nonsignificant differences between the number of colonies obtained.

2.5 | Quantitative analysis of α-amylase activity

Relative extracellular α-amylase activity was quantified in the culture supernatant of strains BAC0352-0355 and BAC0360-0363 using a starch degradation assay. For each strain, an overnight culture was used to inoculate a pre-culture supplemented with chloramphenicol and 1 mmol/L IPTG. Once in exponential growth phase, the pre-culture was back diluted in triplicate into fresh and prewarmed medium also supplemented with chloramphenicol and 1 mmol/L IPTG and grown for 24 hr. Supernatant samples were clarified by centrifugation and 25 μL were mixed in triplicate with 100 μL assay solution (50 mmol/L Tris-HCl, pH 6.8, 25 mmol/L $CaCl_2$, 0.05% [wt/vol] soluble potato starch) and incubated for 30 min at 37°C. 50 μL stop solution (1 mol/L HCl, 0.01% [wt/vol] I_2, 0.1% [wt/vol] KI) was added and absorbance at 620 nm measured. Unpaired *t* tests with Welch's correction were performed to determine two-tailed *p* values and identify statistically significant or nonsignificant differences.

2.6 | Quantitative analysis of GFPmut3 expression detection

Relative fluorescence was quantified in the cultures of strains BAC0348-0351 and BAC0364-0368. For each strain, an overnight culture was used to inoculate a pre-culture supplemented with chloramphenicol and 1 mmol/L IPTG. Once in exponential growth phase, the pre-culture was back diluted into fresh and prewarmed medium also supplemented with chloramphenicol and 1 mmol/L IPTG and grown for 24 hr. The culture fluorescence was measured in samples of 100 μL using the FLUOstar Omega Microplate Reader (BMG LABTECH) in 96-well flat-bottom plates (excitation: 485 nm; emission: 520 nm; gain: 1,000; Greiner). Unpaired *t* tests with Welch's correction were performed to determine two-tailed *p* values and identify statistically significant or nonsignificant differences.

3 | RESULTS

3.1 | Comparison of CRISPR-Cas9 and CRISPR-MAD7 enabled genome editing efficiencies

To compare the gene-editing efficiencies between Cas9 and MAD7 in *B. subtilis*, chromosomally expressed *amyE* and *gfpmut3* genes were selected due to ease of analysis of successfully edited colonies by starch degradation or fluorescence respectively. For both nucleases, a single dDNA with 1 kbp homology arms, either side of the site targeted for modification, was designed to introduce a stop codon at the 5′ of the gene and remove the PAM sites selected based on their proximity (Figure 1a,b).

Cas9 and MAD7 yielded *amyE* knock-out efficiencies of 98% and 93% respectively when the editing plasmids were co-transformed with dDNA to *B. subtilis* 168 (Figure 1c). When knocking out *gfpmut3*, editing efficiencies of 75% and 100% were observed for Cas9 and
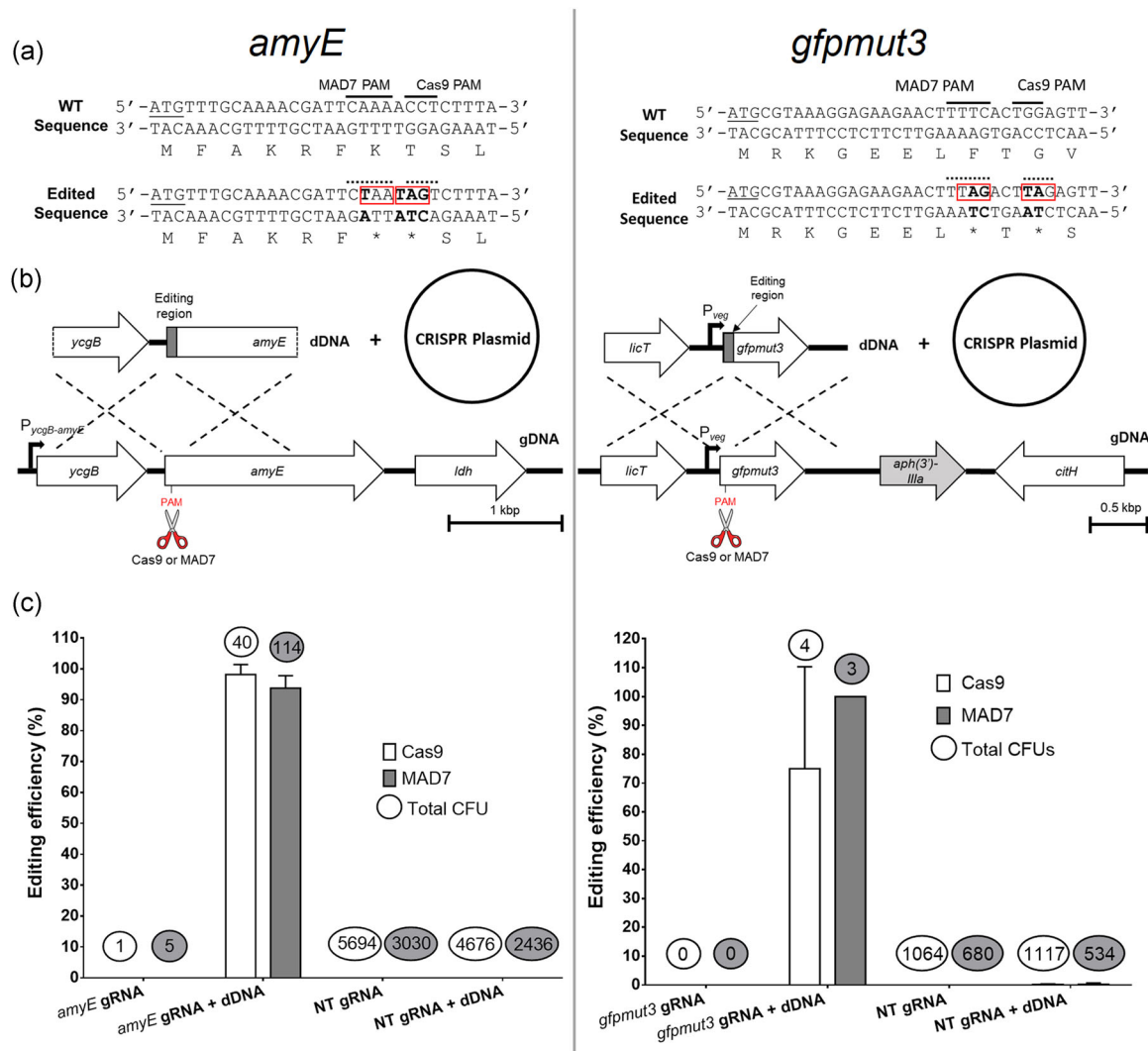
FIGURE 1 CRISPR-Cas9 or CRISPR-MAD7-mediated editing of *amyE* and *gfpmut3*. (a) Non-edited (WT) and edited sequences with their corresponding amino acid sequences (*=stop codon). The targeted PAM sites are indicated for both Cas9 and MAD7. The modified base pairs are highlighted in bold and the introduced stop codons are marked with red boxes. (b) Co-transformational editing approach were the CRISPR plasmid expressing the gRNA and nuclease is transformed alongside a linear editing template (dDNA) containing the editing region. (c) Editing efficiency following co-transformation of *B. subtilis* 168 (*amyE*) or BAC0288 (*gfpmut3*). Bars represent the average editing efficiency obtained following transformation of the targeting or nontargeting (NT) gRNA expression plasmids for each nuclease with or without dDNA (*amyE* targeting: Cas9: pBAC0041; MAD7: pBAC0162. *gfpmut3*: Cas9: pBAC0165; MAD7: pBAC0166. NT: Cas9: pBAC0035; MAD7: pBAC0163). Editing efficiency (%) was determined by observing either starch degradation or fluorescence in the transformation plates. The circled number above each bar indicates the total number of colonies phenotypically screened. Error bars indicate the standard deviation between three independent transformation events. dRNA, donor template DNA; gRNA, guide RNA; WT, wild-type [Color figure can be viewed at wileyonlinelibrary.com]

MAD7 respectively despite the lower transformation efficiency of BAC0288 (Figure 1c). In the absence of dDNA, the DSB catalyzed by either nuclease drastically reduces cell viability and no successfully edited colonies were identified. Following phenotypic analysis, the genotypes of a selected population of the transformants were confirmed by colony PCR and sequencing for both *amyE* and *gfpmut3* (Table S3).

Nontargeting plasmids, containing a gRNA with a random DNA sequence which does not target anywhere in the genome of *B. subtilis* 168 were transformed with and without dDNA for both *amyE* and *gfpmut3* to determine the basal level of editing in the absence of the

DSB induced by a CRISPR nuclease (Figure 1c). A basal level of editing of 2 in 1,117 CFUs and 1 in 534 CFUs was phenotypically detected when the dDNA for *gfpmut3* editing was co-transformed with the Cas9 or MAD7 nontargeting plasmids, respectively. In the case of *amyE*, no edited colonies were detected with the same strategy. This highlights the importance of having both the nuclease and targeting gRNA present to ensure high editing efficiency is obtained due to the counter-selection of unedited colonies. The higher number of colonies analyzed following transformation of the nontargeting plasmids was due to the absence of the selective pressure, against colony formation, in non-edited cells when a targeting gRNA is present.
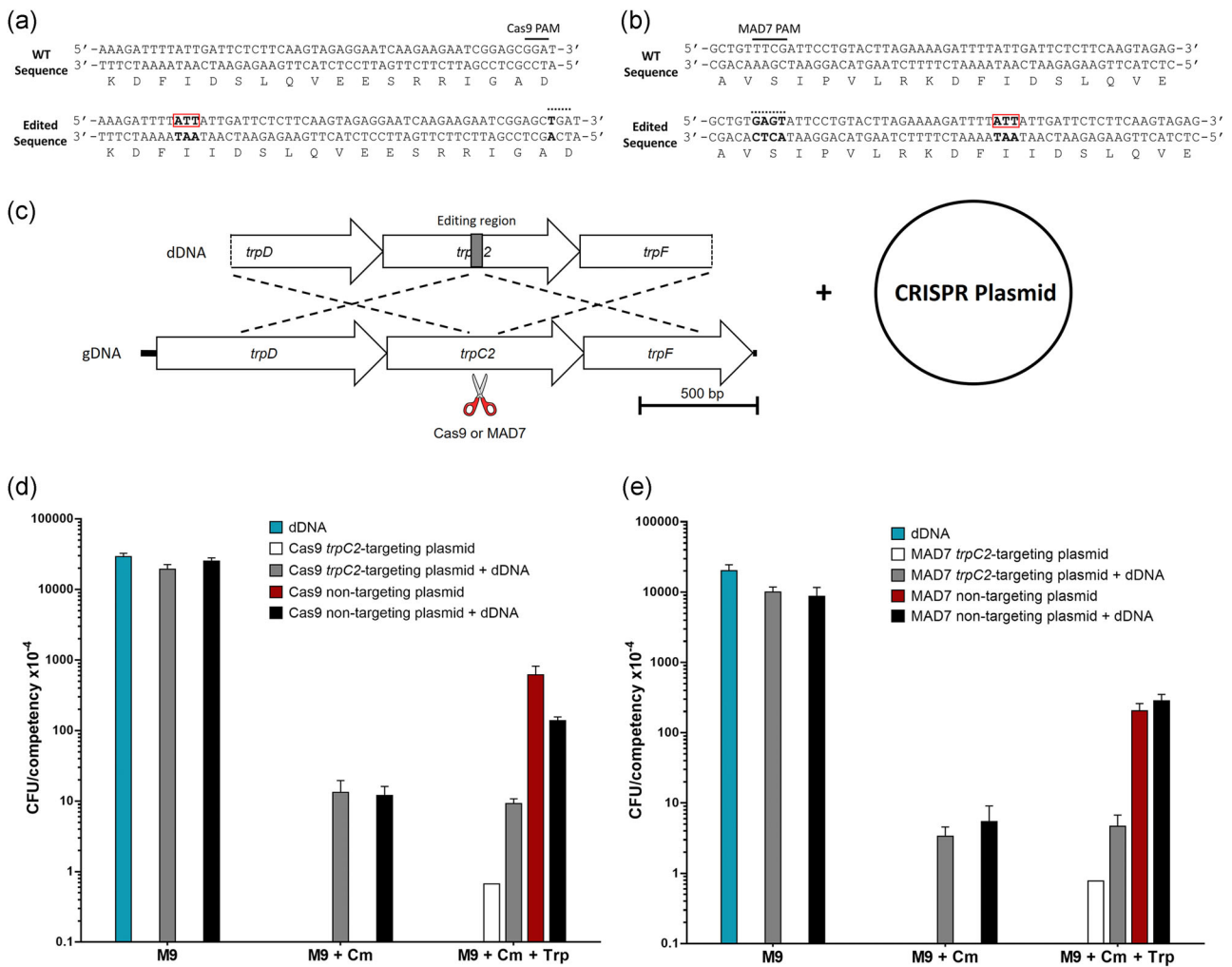
FIGURE 2 Restoration of *B. subtilis* prototrophy using CRISPR-Cas9 and CRISPR-MAD7 for genome editing. (a and b) show the non-edited (WT) and edited sequences for Cas9 and MAD7 editing respectively as well as their corresponding amino acid sequences. The modified base pairs are highlighted in bold and the inserted isoleucine (Ile) codon, adjacent to I110, is marked with red boxes. (c) Co-transformational editing approach were the CRISPR plasmid expressing the gRNA and nuclease is transformed alongside a linear editing template (dDNA) containing the editing region. (d and e) Graphs show the number of transformants following transformations with the indicated combinations of dDNA and targeting (pBAC0185 for Cas9 and pBAC0218 for MAD7) or nontargeting plasmid (pBAC0035 for Cas9 and pBAC0163 for MAD7) to restore *B. subtilis* 168 prototrophy, with Cas9 and MAD7, respectively. Bars represent the average number of colony-forming unit (CFU) normalized by the transformation efficiency of pBAC0035 (Cas9) selected on LB agar supplemented with chloramphenicol or pBAC0163 (MAD7) selected on LB agar supplemented with chloramphenicol and IPTG. Error bars indicate the standard deviation between three independent transformation events. Cm, chloramphenicol; dRNA, donor template DNA; IPTG, isopropyl β-D-1-thiogalactopyranoside; LB, Lysogeny broth; Trp, tryptophan; WT, wild-type [Color figure can be viewed at wileyonlinelibrary.com]

3.2 | Homologous recombination versus DNA double-strand break repair as the driving mechanism for CRISPR genome editing in *B. subtilis* 168

To elucidate the mechanism with which CRISPR-mediated editing takes place in *B. subtilis* 168, we made use of this strain's tryptophan auxotrophy to compare the efficiency in restoring prototrophy when a linear dDNA is transformed on its own, or in the presence of either a Cas9 or MAD7 nontargeting or *trpC2*-targeting plasmid. The linear dDNA, harboring 1 kbp homology regions either side of the site targeted for modification, was designed to simultaneously introduce an additional isoleucine residue adjacent to I110 residue of TrpC2, returning the strain to a prototrophic state, and a synonymous mutation to eliminate

the PAM recognition site and prevent continuous cutting by the *trpC2*-targeting plasmid (Figure 2a,b; Altenbuchner, 2016). By selecting transformants in M9 minimal medium supplemented with or without either chloramphenicol (plasmid selection) or tryptophan, we could clarify whether HR drives genome editing, preventing a DSB, or if the DSB induces DNA repair by HR. As the procedure to induce natural competence utilizes tryptophan within the growth medium throughout, there is no selection for prototrophic cells before the spreading of the transformants on the agar plates.

In the absence of tryptophan, there is not a significant difference in CFU obtained when transforming the linear dDNA to restore tryptophan prototrophy on its own or in the presence of either the *trpC2* targeting or nontargeting plasmids (Figure 2). Furthermore, when cells with restored

prototrophy were also selected in the presence of chloramphenicol, there was no significant difference between the co-transformation of dDNA with either the *trpC2*-targeting or nontargeting CRISPR-Cas9 plasmids (Figure 2). Both these results indicate that HR is the main driving force for CRISPR-Cas9 editing in the presence of dDNA. When M9 was supplemented with tryptophan, the absence of selective pressure for restored prototrophy results in a significantly lower number of CFU when co-transforming the dDNA and the *trpC2*-targeting plasmid compared with the co-transformation of dDNA with the nontargeting plasmid (Figure 2). In this case, the lethal cut induced by the nuclease counterselects the transformants in which HR of dDNA has not occurred. As such, while the high efficiency of HR is the main driving force for genome editing, the nuclease induced DSB is essential to obtain high editing efficiency in *B. subtilis* 168.

3.3 | Engineering of MAD7 to construct and characterize the catalytically inactive dMAD7

3.3.1 | Identification of MAD7 catalytic residues

A pairwise alignment of the amino acid sequences of MAD7 and AsCpf1, confirmed the 31% identity (Figure S2). Previously, it was reported that the catalytic residues of AsCpf1 are Asp908, Glu993, and Asp1263 (Yamano et al., 2016; Zetsche et al., 2015). Asp908 lies in a region of high similarity with MAD7, with residues 905-916 corresponding to MAD7 residues 874-885. AsCpf1 Glu993 does not lie in a region of high homology, however, the alignment revealed that this residue was conserved in MAD7. Finally, the residue corresponding to Asp1263 in AsCpf1 was found in a region on high homology with AsCpf1, with residues 1261–1268 corresponding to MAD7 residues 1211–1218. The corresponding catalytic residues in MAD7 (Asp877, Glu962, and Asp1213) identified by sequence homology (Figure S2) were simultaneously modified to alanine in silico and the corresponding gene *dMAD7* was synthesized.

3.3.2 | dMAD7 lacks the ability to induce a lethal DNA double-strand break

To verify whether the DNA cleavage capacity of MAD7 was removed in the putative dMAD7, the synthesized *dMAD7* gene was used to replace *MAD7* within the *amyE* and *gfpmut3* targeting plasmids pBAC0162 and pBAC0166, respectively. As a control, the well-characterized *dcas9* was used to replace *cas9* in plasmids pBAC0041 and pBAC0165 (Peters et al., 2016; Qi et al., 2013; Westbrook et al., 2016b). Naturally competent *B. subtilis* 168 and BAC0288 were respectively transformed with the *amyE* and *gfpmut3* targeting plasmids with both active and inactive nuclease variants. Triplicate transformations were spread on plates supplemented with chloramphenicol and IPTG to ensure nuclease expression. The average number of CFUs obtained for each set of transformations (Table 1) indicates that the engineered dMAD7 does

TABLE 1 Average number of transformants (CFU) obtained following triplicate transformation reactions of naturally competent *B. subtilis* 168 and BAC0288 with 200 ng of Cas9, dCas9, MAD7, and dMAD7 plasmids

Parental strain	Target	Plasmid	Nuclease	Average CFU obtained
B. subtilis 168	*amyE*	pBAC0041	Cas9	0.3
		pBAC0184	dCas9	898
		pBAC0162	MAD7	1.7
		pBAC0188	dMAD7	1,248
BAC0288	*gfpmut3*	pBAC0165	Cas9	0
		pBAC0195	dCas9	392
		pBAC0166	MAD7	0.7
		pBAC0190	dMAD7	343

Abbreviation: CFU, colony-forming unit.

not catalyze DSB of DNA since it does not cause the reduced viability observed for the catalytically active nuclease.

3.3.3 | dMAD7 retains DNA binding capacity to enable CRISPRi

Extracellular α-amylase activity was quantified in strains expressing dMAD7 targeting five PAM sites (5′-TTTN-3′) at the 5′ end of *amyE*, two on the template strand and three on the nontemplate strand. The results were directly compared with strains expressing dCas9 targeting *amyE* +25 bases downstream of the start codon. Strains expressing nontargeting dMAD7 and dCas9 plasmids were used as the negative controls for downregulation (Figure 3a,b).

The results confirm that dCas9-mediated CRISPRi is highly efficient with a 99.4% reduction in α-amylase activity, while dMAD7-mediated CRISPRi appears less efficient, ranging from 59.3% to 51.5% activity reduction depending on the gRNA and PAM site sequence. The gRNA targeting the PAM site TTTG +21 bases from the start codon did not exhibit significantly reduced levels of activity. As this PAM sequence was the same as others where CRISPRi was successful, and the GC % of the protospacer (28.6%) is similar to the one targeting the PAM site +4 (33.3%), we hypothesize the cause of this lowered efficiency is due to secondary structure within the gRNA, as has previously been reported for Cas9 (Thyme, Akhmetova, Montague, Valen, & Schier, 2016; Xu, Lian, Jia, Li, & Huang, 2017).

To further investigate the capacity of dMAD7 for CRISPRi, the *gfpmut3* gene in strain BAC0288 was targeted. Here, six PAM sites (three on each strand) where targeted with the 5′-YTTN-3′ PAM sequence recommended by Inscripta (Figure 3c). dMAD7 was targeted to the 5′ end of *gfpmut3* and fluorescence was compared with strains expressing dCas9 targeting *gfpmut3* +27 bases downstream of the start codon. Strains expressing nontargeting dMAD7 and dCas9 plasmids were used as negative controls for
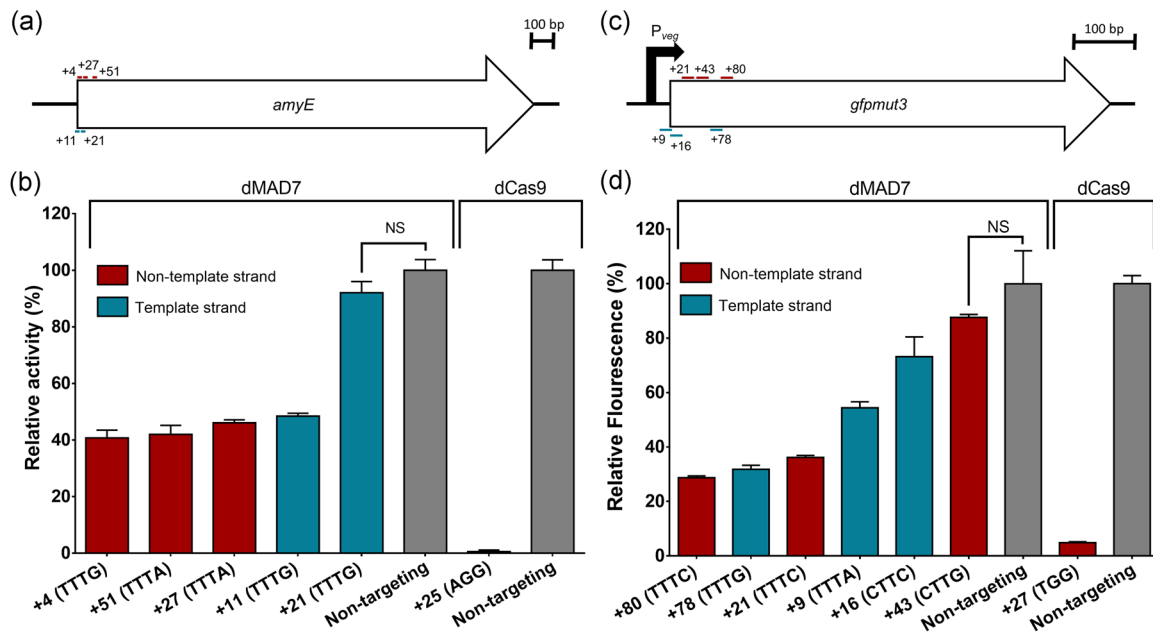
FIGURE 3 Relative α-amylase activity and GFPmut3 fluorescence following dCas9 and dMAD7-mediated CRISPRi. (a and c) Schematic diagrams of gRNA binding sites for dMAD7 within *amyE* and *gfpmut3* respectively. Values represent the distance of each targeted PAM site from the start codon on either the template (blue) or non-template (red) DNA strand. (b) Bar graph represents the extracellular α-amylase activity normalized by $OD_{600 nm}$ relative to the nontargeting gRNA control for either dMAD7 or dCas9, after 24 hr of growth. The horizontal axis indicates the PAM site targeted by each gRNA for both dMAD7 and dCas9 and its distance to the *amyE* start codon (+4: BAC0360; +51: BAC0363; +27: BAC0362; +11: BAC0361; +21: BAC0355; +25: BAC0353). Red and blue bars correspond to PAM sites on the non-template and template strands, respectively. Gray bars represent nontargeting controls (dMAD7: BAC0354; dCas9: BAC0352). (d) Bar graph represents the fluorescence intensity normalized by $OD_{600 nm}$ relative to the nontargeting gRNA control for either dMAD7 or dCas9, after 24 hr of growth. The horizontal axis indicates the PAM site targeted by each gRNA for both dMAD7 and dCas9 and its distance to the *gfpmut3* start codon (+80: BAC0368; +78: BAC0367; +21: BAC0351; +9: BAC0364; +16: BAC0365; +43: BAC0366; +27: BAC0349). Red and blue bars correspond to PAM sites on the non-template and template strands, respectively. Gray bars represent the nontargeting controls (dMAD7: BAC0350; dCas9: BAC0348). Error bars indicate the standard deviation between three biological replicates. Two-tailed *p* values following unpaired *t* test with Welch's correction. gRNA, guide RNA; NS, not significant [Color figure can be viewed at wileyonlinelibrary.com]

downregulation (Figure 3d). Here, a broader effect on expression was observed for dMAD7 with statistically significant CRISPRi efficiencies ranging from 71.3% to 26.8%. Once again, the *gfpmut3* targeting dCas9 control exhibited highly efficient CRISPRi with a 95.1% reduction in expression. This difference in efficiency may indicate that further modifications to dMAD7 could be made to increase its ability to bind DNA efficiently.

3.3.4 | Multiplexed CRISPRi of *amyE* and *gfpmut3* with dMAD7

To increase the efficiency of dMAD7 transcriptional downregulation, multiplexed targeting, where more than one gRNA is utilized at a time, was tested. gRNA arrays were inserted in the same manner as single gRNAs, with the final array designed with the dMAD7 handle direct repeat at both the 3′ and 5′ ends, as well as between the inserted protospacers.

Additive downregulation of *amyE* was tested by targeting PAM sites at +4 TTTG and +51 TTTA in strain BAC0377 (Figure 4b). Similarly,

gfpmut3 was analyzed by targeting PAM sites at +80 TTTC and +21 TTTG in strain BAC0380 (Figure 4b). These were compared with the nontargeting dMAD7 control strain BAC0350, as well as the single gRNA, *amyE* or *gfpmut3* targeting dMAD7 strains BAC0381, BAC0382, BAC0351, and BAC0368. To ensure the gRNA array was matured from a single transcript into single gRNA units, strain BAC0378, carrying a gRNA array to target *amyE* +4 TTTG and *gfpmut3* +80 TTTC was analyzed for transcriptional interference of both targets (Figure 4c).

The results show when *amyE* and *gfpmut3* were simultaneously targeted the downregulation of both genes was found to be similar to when only one was targeted for CRISPRi (Figure 4c). As such, the gRNA array was correctly matured to single gRNAs and there is no significant competition between the two gRNAs for dMAD7-mediated CRISPRi.

When two gRNAs are combined to target either *gfpmut3* or *amyE*, the measured downregulation is not cumulative. As the BAC0378 multiplexing results indicate no significant competition between the gRNAs for dMAD7, it is thought that there is a potential steric hindrance between the protospacer-dMAD7 complexes used to simultaneously target each reporter.
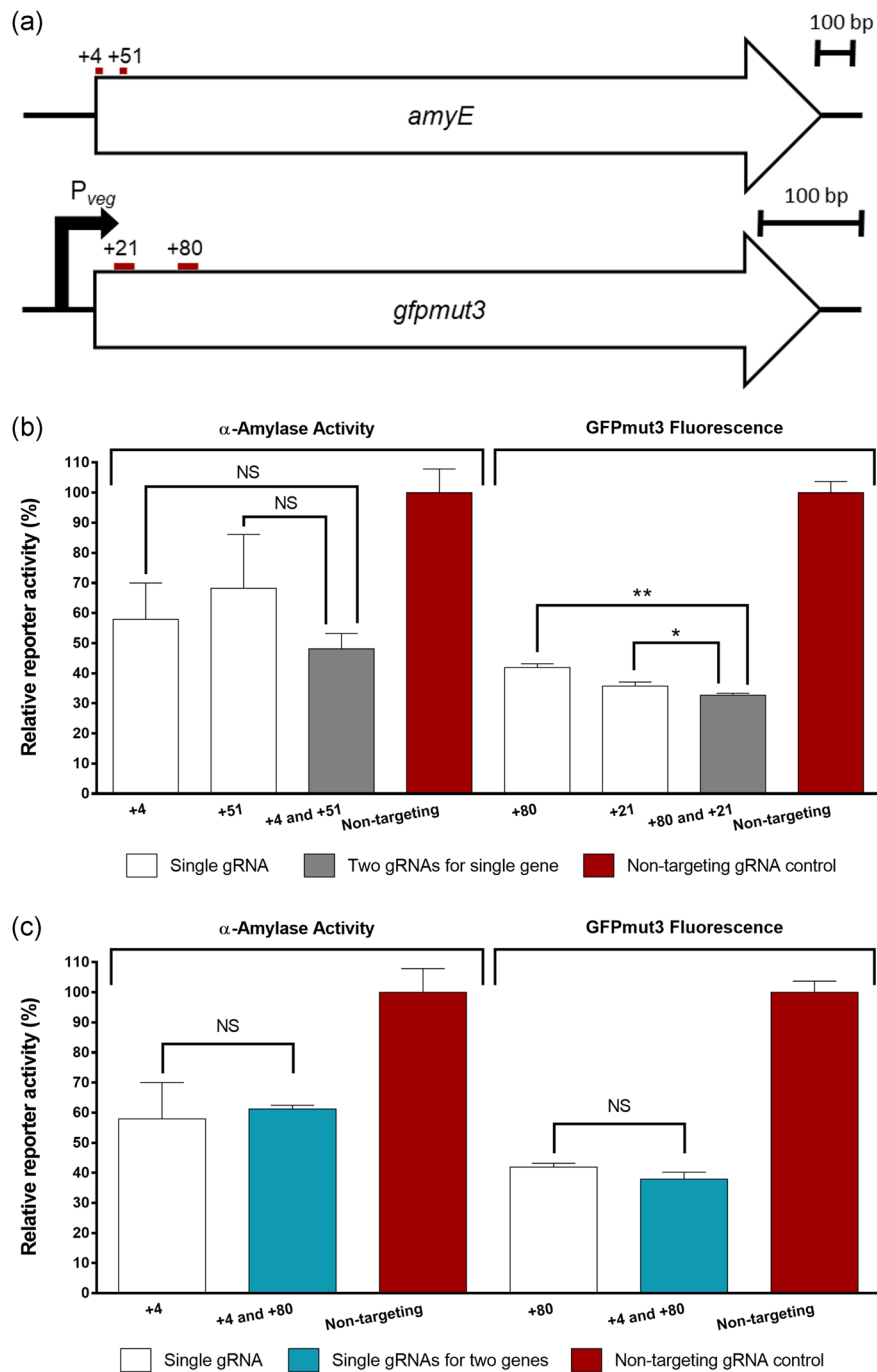
FIGURE 4 Relative α-amylase activity and GFPmut3 fluorescence following dMAD7-mediated multiplexing CRISPRi in BAC0288. (a) Schematic diagrams of gRNA binding sites for dMAD7 within *amyE* and *gfpmut3*. Values represent the distance of each targeted PAM site from the start codon on the non-template DNA strand. (b) Investigation for an additive multiplexed CRISPRi effect when two gRNAs target a single gene. (c) Investigation for a multiplexed CRISPRi effect when two gRNAs target different genes within the same strain. Bars represent extracellular α-amylase activity, or GFPmut3 fluorescence intensity, normalized by $OD_{600 nm}$, relative to the nontargeting gRNA control strain, after 24 hr of growth. The horizontal axis indicates the targeted PAM site(s) distance to the *amyE* or *gfpmut3* start codon (Strains used: +4: BAC0381; +51: BAC0382;+4 and +51: BAC0377; +4 and +80: BAC0378; +80: BAC0368; +21: BAC0351; +80 and +21: BAC0380). White bars indicate strains in which a single gRNA is utilized to target a single gene. Gray bars indicate strains in which the effect of two gRNAs on a single gene is investigated. Blue bars indicate BAC0378 in which the effect of single gRNAs on two different genes is investigated. Red bars indicate the negative control strain, BAC0350, in which a nontargeting gRNA is expressed alongside *dMAD7*. Error bars indicate the standard deviation between three biological replicates. *$p < .05$; **$p < .01$. Two-tailed *p* values were derived following unpaired *t* test with Welch's correction. gRNA, guide RNA; NS, not significant [Color figure can be viewed at wileyonlinelibrary.com]

4 | DISCUSSION

We have exemplified the first reported use of the CRISPR-associated nuclease MAD7 free for all commercial or academic research in the Gram-positive model organism, *B. subtilis*. The MAD7-mediated genome editing efficiency determined by targeting *amyE* (93%) and *gfpmut3* (100%) was comparable to the commonly used Cas9 nuclease. This indicates that MAD7 is a viable alternative to Cas9 for strain development of the industrial workhorse *B. subtilis*. These results also indicate that the killing efficiency of MAD7 (*amyE*: 99.84%; *trpC2*: 99.62%) in *B. subtilis*, determined by the total number of CFUs following transformation with targeting versus nontargeting plasmids only, was similar to that of Cas9 (*amyE*: 99.98%; *trpC2*: 99.89%). It is hypothesized that, due to the strong selection for survival, these "escaper" colonies may harbor mutations deactivating the killing capacity of the CRISPR systems. Such mutations may occur within the editing plasmid, or on the chromosome at the PAM site or the first 10–12 nt of the gRNA protospacer (known as the seed region) within which any mutations cause a severely deleterious effect on cleavage efficiency (Jiang, Bikard, Cox, Zhang, & Marraffini, 2013; Jinek et al., 2012).

We have provided evidence that, in *B. subtilis* 168, CRISPR-Cas9 and CRISPR-MAD7 genome editing efficiency is driven primarily by HR of dDNA preventing the lethal Cas9 or MAD7-induced DNA DSB, rather than HDR following the DSB. Mougiakos et al. reported the endogenous HR machinery within *Bacillus smithii* incorporating plasmid-borne dDNA while Cas9 was inactive at ≥42°C. Counterselection of the cells which had not undergone HR was then performed at 37°C where the Cas9 was once again functional. Here we have shown HR as the driving mechanism under temperatures where the nuclease is active and growth is optimal (Mougiakos et al., 2017). The presence of the CRISPR-Cas9 or CRISPR-MAD7 system was not required to detect successful HR due to prototrophic selection on M9 minimal medium. However, where such a selection is not possible, the CRISPR-Cas9 or CRISPR-MAD7 systems act as a powerful counterselection for unedited cells. Additionally, the editing efficiency reported here with pBAC0041 and dDNA (Figure 1) in the presence of IPTG for Cas9 expression induction (91%) is similar to that previously reported in the absence of IPTG (89.2%; Price et al., 2019). Thus, editing rates are decoupled from Cas9 expression levels with leaky P_{grac} promoter activity being sufficient to induce the lethal DSB. Moreover, as the natural competency master regulator ComK activates transcription of the primary component of HR, *recA*, and DNA uptake is single-stranded, yielding a substrate with which RecA can bind, HR can readily proceed at the target site before the DSB taking place (Cheo, Bayles, & Yasbin, 1993; Dubnau, 1999).

Furthermore, a catalytically inactive variant of MAD7 was engineered retaining its ability to bind DNA in the presence of a DNA-targeting gRNA. Our data highlights the importance of testing multiple gRNA sequences when optimizing the MAD7-mediated downregulation of a target gene. The level of downregulation is likely influenced by a combination of factors, such as PAM site sequence, gRNA binding efficiency, GC % of the protospacer, and gRNA secondary structure (Labun et al., 2016; Thyme et al., 2016; Wilson, O'Brien, & Bauer, 2018; Zetsche et al., 2015). Interestingly, the significance of gRNA selection does not seem to be as great when preforming MAD7-mediated editing compared to CRISPRi. The *amyE* +21 targeting PAM site resulted in 98% editing efficiency while only showing a 7.9% decrease of α-amylase activity when preforming CRISPRi with dMAD7. This is likely because the nuclease DSB is a single event whereas CRISPRi requires a stable and continuous interaction between the nuclease and targeted coding sequence for efficient transcriptional downregulation. Multiplexed targeting of dMAD7 to an endogenous and heterologous gene target was exemplified, with no detectable competition between gRNAs on the pool of expressed dMAD7 when compared to strains with only a single gRNA. It is feasible that technologies developed were effector proteins are fused to dCas9 for pathway optimization or in vivo mutagenesis could be adapted for use with dMAD7 further expanding its potential (Bikard et al., 2013; Wang et al., 2018; Yang et al., 2018).

An attractive feature of MAD7 is its freedom to use for industrial R&D and commercial strain construction (provided the final strain does not retain the MAD7 nuclease (Inscripta, 2019b)). This has the capacity to disrupt the slow commercial uptake of genome editing technologies allowing the use of MAD7 in sectors that were put off by licensing and royalty fees associated with for instance Cas9 and Cpf1 CRISPR nucleases, such as large-scale fermentation biotechnology.

ORCID

Marcus A. Price http://orcid.org/0000-0002-7435-873X
Susan J. Rosser http://orcid.org/0000-0002-2560-6485

REFERENCES

Adli, M. (2018). The CRISPR tool kit for genome editing and beyond. *Nature Communications*, 9, 1911. https://doi.org/10.1038/s41467-018-04252-2

Altenbuchner, J. (2016). Editing of the *Bacillus subtilis* genome by the CRISPR-Cas9 system. *Applied and Environmental Microbiology*, 82(17), 5421–5427. https://doi.org/10.1128/AEM.01453-16

Anagnostopoulos, C., & Spizizen, J. (1961). Requirements for transformation in *Bacillus subtilis. Journal of Bacteriology*, 81(5), 741–746.

Bennallack, P. R., Burt, S. R., Heder, M. J., Robison, R. A., & Griffitts, J. S. (2014). Characterization of a novel plasmid-borne thiopeptide gene cluster in *Staphylococcus epidermidis* strain 115. *Journal of Bacteriology*, 196(24), 4344–4350. https://doi.org/10.1128/JB.02243-14

Bikard, D., Jiang, W., Samai, P., Hochschild, A., Zhang, F., & Marraffini, L. A. (2013). Programmable repression and activation of bacterial gene expression using an engineered CRISPR-Cas system. *Nucleic Acids Research*, 41(15), 7429–7437. https://doi.org/10.1093/nar/gkt520

Bisicchia, P., Botella, E., & Devine, K. M. (2010). Suite of novel vectors for ectopic insertion of GFP, CFP and IYFP transcriptional fusions in single copy at the *amyE* and *bglS* loci in *Bacillus subtilis. Plasmid*, 64(3), 143–149. https://doi.org/10.1016/j.plasmid.2010.06.002

Bryksin, A. V., & Matsumura, I. (2010). Overlap extension PCR cloning: A simple and reliable way to create recombinant plasmids. *Biotechniques*, *48*(6), 463–465. https://doi.org/10.2144/000113418

Burby, P. E., & Simmons, L. A. (2017). MutS2 promotes homologous recombination in *Bacillus subtilis*. *Journal of Bacteriology*, *199*(2), https://doi.org/10.1128/JB.00682-16

Che, A., Knight, T., Canton, B., Kelly, J., & Shetty, R. (2015). Iti Scotland Limited. *United States Patent No. US 8,999,679 B2*. United States of America.

Cheo, D. L., Bayles, K. W., & Yasbin, R. E. (1993). Elucidation of regulatory elements that control damage induction and competence induction of the *Bacillus subtilis* SOS system. *Journal of Bacteriology*, *175*(18), 5907–5915. https://doi.org/10.1128/jb.175.18.5907-5915.1993

Dicarlo, J. E., Norville, J. E., Mali, P., Rios, X., Aach, J., & Church, G. M. (2013). Genome engineering in *Saccharomyces cerevisiae* using CRISPR-Cas systems. *Nucleic Acids Research*, *41*(7), 4336–4343. https://doi.org/10.1093/nar/gkt135

Dubnau, D. (1999). DNA uptake in bacteria. *Annual Review of Microbiology*, *53*(1), 217–244. https://doi.org/10.1146/annurev.micro.53.1.217

Harwood, C. R., & Cutting, S. M. (1990). *Molecular Biological Methods for Bacillus*. John Wiley & Sons.

Inscripta, I. (2019a). Introducing MAD7 | Inscripta. Retrieved from https://www.inscripta.com/madzymes/

Inscripta, I. (2019b). MADzyme FAQs | Inscripta. Retrieved from https://www.inscripta.com/madzymes/faq/

Jakočiūnas, T., Jensen, M. K., & Keasling, J. D. (2015). CRISPR/Cas9 advances engineering of microbial cell factories. *Metabolic Engineering*, *34*, 44–59. https://doi.org/10.1016/j.ymben.2015.12.003

Jakutyte-Giraitiene, L., & Gasiunas, G. (2016). Design of a CRISPR-Cas system to increase resistance of *Bacillus subtilis* to bacteriophage SPP1. *Journal of Industrial Microbiology & Biotechnology*, *43*(8), 1183–1188.

Jiang, W., Bikard, D., Cox, D., Zhang, F., & Marraffini, L. a (2013). RNA-guided editing of bacterial genomes using CRISPR-Cas systems. *Nature Biotechnology*, *31*(3), 233–239. https://doi.org/10.1038/nbt.2508

Jinek, M., Chylinski, K., Fonfara, I., Hauer, M., Doudna, J. A., & Charpentier, E. (2012). A programmable dual-RNA—Guided DNA endonuclease in adaptive bacterial immunity. *Science*, *337*, 816–822. https://doi.org/10.1126/science.1225829

Labun, K., Montague, T. G., Gagnon, J. A., Thyme, S. B., & Valen, E. (2016). CHOPCHOP v2: A web tool for the next generation of CRISPR genome engineering. *Nucleic Acids Research*, *44*(W1), W272–W276. https://doi.org/10.1093/nar/gkw398

Liu, D., Huang, C., Guo, J., Zhang, P., Chen, T., Wang, Z., & Zhao, X. (2019). Development and characterization of a CRISPR/Cas9n-based multiplex genome editing system for *Bacillus subtilis*. *Biotechnology for Biofuels*, *12*(1), 197. https://doi.org/10.1186/s13068-019-1537-1

Lu, Z., Yang, S., Yuan, X., Shi, Y., Ouyang, L., Jiang, S., & Zhang, G. (2019). CRISPR-assisted multi-dimensional regulation for fine-tuning gene expression in *Bacillus subtilis*. *Nucleic Acids Research*, 13. https://doi.org/10.1093/nar/gkz072

Montague, T. G., Cruz, J. M., Gagnon, J. A., Church, G. M., & Valen, E. (2014). CHOPCHOP: A CRISPR/Cas9 and TALEN web tool for genome editing. *Nucleic Acids Research*, *42*(W1), W401–W407. https://doi.org/10.1093/nar/gku410

Mougiakos, I., Bosma, E. F., Weenink, K., Vossen, E., Goijvaerts, K., Van Der Oost, J., & Van Kranenburg, R. (2017). Efficient genome editing of a facultative thermophile using mesophilic spCas9. *ACS Synthetic Biology*, *6*(5), 849–861. https://doi.org/10.1021/acssynbio.6b00339

Peng, F., Wang, X., Sun, Y., Dong, G., Yang, Y., Liu, X., & Bai, Z. (2017). Efficient gene editing in *Corynebacterium glutamicum* using the CRISPR/Cas9 system. *Microbial Cell Factories*, *16*(1), 201. https://doi.org/10.1186/s12934-017-0814-6

Peters, J. M., Colavin, A., Shi, H., Czarny, T. L., Larson, M. H., Wong, S., & Gross, C. A. (2016). A comprehensive, CRISPR-based functional analysis of essential genes in bacteria. *Cell*, *165*(6), 1493–1506. https://doi.org/10.1016/j.cell.2016.05.003

Price, M. A., Cruz, R., Baxter, S., Escalettes, F., & Rosser, S. J. (2019). CRISPR-Cas9 *In Situ* engineering of subtilisin E in *Bacillus subtilis*. *PLoS One*, *14*(1), https://doi.org/10.1371/journal.pone.0210121

Qi, L. S., Larson, M. H., Gilbert, L. A., Doudna, J. A., Weissman, J. S., Arkin, A. P., & Lim, W. A. (2013). Repurposing CRISPR as an RNA-guided platform for sequence-specific control of gene expression. *Cell*, *152*(5), 1173–1183. https://doi.org/10.1016/j.cell.2013.02.022

Sambrook, J., & Russell, R. W. (2001). Molecular cloning: A laboratory manual. 4th Ed.

Shuman, S., & Glickman, M. S. (2007). Bacterial DNA repair by non-homologous end joining. *Nature Reviews Microbiology*, *5*(11), 852–861. https://doi.org/10.1038/nrmicro1768

Thyme, S. B., Akhmetova, L., Montague, T. G., Valen, E., & Schier, A. F. (2016). Internal guide RNA interactions interfere with Cas9-mediated cleavage. *Nature Communications*, *7*(1), https://doi.org/10.1038/ncomms11750

Wang, Y., Liu, Y., Liu, J., Guo, Y., Fan, L., Ni, X., & Ma, Y. (2018). MACBETH: Multiplex automated *Corynebacterium glutamicum* base editing method. *Metabolic Engineering*, *47*, 200–210. https://doi.org/10.1016/j.ymben.2018.02.016

Westbrook, A. W., Moo-Young, M., & Chou, C. P. (2016a). Development of a CRISPR-Cas9 tool kit for comprehensive engineering of *Bacillus subtilis*. *Applied and Environmental Microbiology*, *82*(16), 4876–4895. https://doi.org/10.1128/AEM.01159-16

Westbrook, A. W., Moo-Young, M., & Chou, C. P. (2016b). Development of a CRISPR-Cas9 toolkit for comprehensive engineering of *Bacillus*. *Applied and Environmental Microbiology*, *82*(16), 4876–4895.

Wierson, W. A., Simone, B. W., Warejoncas, Z., Mann, C., Welker, J. M., Gendron, W. A. C., & Essner, J. J. (2019). Expanding the CRISPR toolbox with ErCas12a in zebrafish and human cells. *BioRxiv*, https://doi.org/10.1101/650515

Wilson, L. O. W., O'Brien, A. R., & Bauer, D. C. (2018). The current state and future of CRISPR-Cas9 gRNA design tools. *Frontiers in Pharmacology*, *9*, 749. https://doi.org/10.3389/fphar.2018.00749

Xu, J., Lian, W., Jia, Y., Li, L., & Huang, Z. (2017). Optimized guide RNA structure for genome editing via Cas9. *Oncotarget*, *8*(55), 94166–94171. https://doi.org/10.18632/oncotarget.21607

Yamano, T., Nishimasu, H., Zetsche, B., Ishitani, R., Zhang, F., Correspondence, O. N., & Nureki, O. (2016). Crystal structure of Cpf1 in complex with guide RNA and target DNA. *Cell*, *165*, 949–962. https://doi.org/10.1016/j.cell.2016.04.003

Yang, L., Zhang, X., Wang, L., Yin, S., Zhu, B., Xie, L., & Li, D. (2018). Increasing targeting scope of adenosine base editors in mouse and rat embryos through fusion of TadA deaminase with Cas9 variants. *Protein & Cell*, *9*(9), 814–819. https://doi.org/10.1007/s13238-018-0568-x

Zetsche, B., Gootenberg, J. S., Abudayyeh, O. O., Slaymaker, I. M., Makarova, K. S., Essletzbichler, P., & Zhang, F. (2015). Cpf1 is a single RNA-guided endonuclease of a class 2 CRISPR-cas system. *Cell*, *163*(3), 759–771. https://doi.org/10.1016/j.cell.2015.09.038

Zhang, K., Duan, X., & Wu, J. (2016). Multigene disruption in undomesticated *Bacillus subtilis* ATCC 6051a using the CRISPR/Cas9 system. *Scientific Reports*, *6*(27943), 1–11.

Zhang, X. Z., Yan, X., Cui, Z. L., Hong, Q., & Li, S. P. (2006). *mazF*, a novel counter-selectable marker for unmarked chromosomal manipulation in *Bacillus subtilis*. *Nucleic Acids Research*, *34*(9), e71. https://doi.org/10.1093/nar/gkl358

Zhu, X., Zhao, D., Qiu, H., Fan, F., Man, S., Bi, C., & Zhang, X. (2017). The CRISPR/Cas9-facilitated multiplex pathway optimization (CFPO) technique and its application to improve the *Escherichia coli* xylose

utilization pathway. *Metabolic Engineering, 43,* 37–45. https://doi.org/10.1016/j.ymben.2017.08.003

SUPPORTING INFORMATION

Additional supporting information may be found online in the Supporting Information section.